

Bayesian inversion of GPR waveforms for uncertainty-aware sub-surface material characterization

Ishfaq Aziz¹, Elahe Soltanaghai², Adam Watts³, Mohamad Alipour⁴

¹Civil and Environmental Engineering, University of Illinois Urbana Champaign (Corresponding author, ishfaqa2@illinois.edu)

²Computer Science, University of Illinois Urbana Champaign

³Pacific Wildland Fire Sciences Laboratory, United States Forest Service

⁴Civil and Environmental Engineering, University of Illinois Urbana Champaign

Abstract

Accurate estimation of sub-surface properties like moisture content and depth of layers is crucial for applications spanning sub-surface condition monitoring, precision agriculture, and effective wildfire risk assessment. Soil in nature is often covered by overlaying surface material, making its characterization using conventional methods challenging. In addition, the estimation of the properties of the overlaying layer is crucial for applications like wildfire assessment. This study thus proposes a Bayesian model-updating-based approach for ground penetrating radar (GPR) waveform inversion to predict sub-surface properties like the moisture contents and depths of the soil layer and overlaying material accumulated above the soil. The dielectric permittivity of material layers were predicted with the proposed method, along with other parameters, including depth and electrical conductivity of layers. The proposed Bayesian model updating approach yields probabilistic estimates of these parameters that can provide information about the confidence and uncertainty related to the estimates. The methodology was evaluated for a diverse range of experimental data collected through laboratory and field investigations. Laboratory investigations included variations in soil moisture values and depth of the top layer (or overlaying material), and the field investigation included measurement of field soil moisture for sixteen days. The results demonstrated predictions consistent with time-domain reflectometry (TDR) measurements and conventional gravimetric tests. The top layer depth could also be predicted with reasonable accuracy. The proposed method provides a promising approach for uncertainty-aware sub-surface parameter estimation that can enable decision-making for risk assessment across a wide range of applications.

Keywords: ground penetrating radar (GPR), full-waveform inversion (FWI), FDTD, bayesian model updating, optimization, soil and fuel moisture.

1. Introduction

The determination of sub-surface properties and soil water content is pivotal in a multitude of domains like efficient agriculture (Liu et al., 2016), infrastructure planning and condition monitoring (Kalogeropoulos, 2011; Kaplanvural, 2023), water resource management (Srivastava, 2017), and environmental conservation. It helps optimize irrigation, prevent

droughts and floods, protect ecosystems, and inform sustainable land use planning. In potential wildfire risk areas, measuring soil moisture levels enables the identification of wildfire hotspots (Ambadan et al., 2020), likelihood of wildfire occurrence (Jensen et al., 2018), assessment of the size of a wildfire (Krueger et al., 2015), all of which are significant in effective wildfire management. Furthermore, during prescribed burning to reduce wildland fuel hazards, soil moisture content can impact the survival of vital microorganisms, which in turn can affect plant growth (Dunn et al., 1985). The importance of soil moisture content in such diversified applications makes the accurate and efficient determination of soil moisture content essential.

In many cases, the soil layer is covered with layers of woody material such as live or dead vegetation, dry leaves, branches, and decomposed organic materials. This makes the direct measurement of soil moisture through the top layer challenging. Furthermore, in applications such as forest fire risk assessment and post-fire effects, rapid assessment of the depth and moisture of the top woody layer is of utmost importance (Rao et al., 2020). In such cases, the top layer acts as fuel for wildfires, and the depth and moisture content of this fuel layer directly affect the spread and aftereffects of wildfires on the ecosystem (García et al., 2020). Surface fuel measurements are primary inputs to fuel mapping systems (Alipour et al., 2023; Cova et al., 2023; Shaik et al., 2023; Prichard et al., 2019; Stavros et al., 2018; Falkowski et al., 2005). Moreover, inaccurate characterization of fuels results in errors, sometimes even more than 100%, in predicting fire perimeter and burned area (Mutlu et al., 2008), limiting operational decision-making in wildland fire response and pre-fire treatments such as prescribed burns. Hence, measuring the properties of the top layer in addition to that of the soil underneath is of immense importance.

Current practices for determining sub-surface moisture typically use gravimetric analysis, which involves labor-intensive and time-consuming collection and weighing of soil samples before and after oven-drying, or by using different soil sensors that measure properties like resistance, capacitance, and electromagnetic (EM) wave propagation speed. Examples of such sensors are resistive and capacitive sensors and time-domain sensors, to name a few. Resistive soil sensors are less reliable due to degradation and are not recommended for farms, while capacitive sensors are preferred for their durability and accuracy in agricultural contexts (Josephson et al., 2021). Time-domain sensors, like Time Domain Reflectometry (TDR) sensors, offer high accuracy but are relatively costly and hard to deploy, power, and maintain. More importantly, these sensors are only amenable to measure moisture in soil, excluding a top layer of organic material over it.

To address these challenges, in this paper, we investigate the use of ground penetrating radar (GPR) to simultaneously evaluate soil and organic top layer moisture while also estimating the depth of the organic material accumulation. As shown in Figure 1, a GPR antenna sends an electromagnetic wave through a transmitter (T_x) and receives a reflected wave through a

receiver (R_x). The received waveform is a one-dimensional signal called an A-scan (Figure 1b), which can also be viewed by transforming it into an amplitude envelope (Figure 1c). These scan data from radar surveys are used for non-destructive evaluation (He et al., 2023), sub-surface material inspection (Wickramanayake et al., 2022), under canopy biomass sensing (Sinchi et al., 2023); surface water sensing (Serbin et al., 2005), mapping buried glacier ice (Brandt et al., 2007) and many other applications by manual interpretation or by automated and semi-automated implementations like machine learning, surrogate modeling, and full-waveform inversion (FWI).

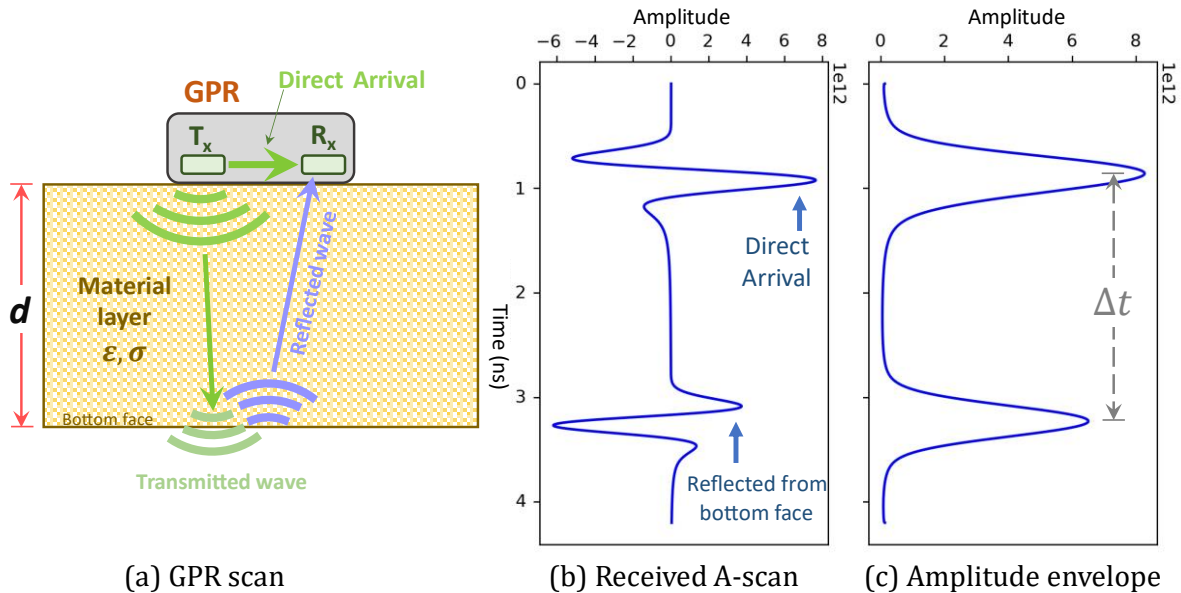


Figure 1: Schematic of GPR measurement and received waveform.

This study contributes to FWI, which is a widely used computational technique that utilizes complete waveform information, including amplitude, phase, and frequency content of a signal, to provide detailed insights into the subsurface properties, such as electrical permittivity, acoustic impedance, electrical conductivity, or material depth. Researchers have used FWI of radar data for a wide range of applications, which include estimating the hydraulic properties of soil (Yu et al., 2022), moisture content of building materials (Klewe et al., 2021), reconstruction of tunnel lining defects (Feng et al., 2019), monitoring cement setting time (Xie et al., 2022), inspecting tree trunk defects (Feng et al., 2023), hydraulic aquifer characterization (Haruzi et al., 2022), as well as soil moisture mapping (Wu et al., 2019, Wu et al., 2022). Most of the previous studies on soil moisture mapping estimate moisture content of soil only without considering the effect of organic layers on top of the soil. For most applications related to environmental sensing, an accumulated layer of material, is often found on top of soil (e.g., on a forest floor). Hence, a method for accurate soil moisture estimation in the presence of the top layer is necessary. The depth of the layer of material on top may also change over time, and the estimation of this depth (cover depth) is also important for applications like wildfire risk assessment (Naderpour et al., 2021). Hence, this study uses

waveform inversion for the estimation of soil moisture with the presence of a top material layer as well as for the estimation of the depth of the top layer. Furthermore, the top layer above the soil may be formed of materials of different degrees of coarseness and densities. Thus, moisture estimation with the presence of different top-layer materials having varying degrees of coarseness is investigated and presented in this study. Finally, most existing studies offer a deterministic estimation of soil moisture with little consideration of the uncertainties arising from sensors, target layers, as well as environmental conditions. However, soil and the organic top layer have considerably heterogeneous and stochastic properties, resulting in intrinsic uncertainties that need to be accounted for. This work presents an uncertainty-aware method for soil and organic top-layer parameter estimations that complements the estimations with a measure of uncertainty.

1.1. Related Works

To estimate sub-surface moisture, the primary target parameter estimated in the literature is the dielectric permittivity due to its high correlation with moisture content (Topp et al., 1980). Permittivity refers to a material's capacity to retain an electric charge. The widely employed dielectric permittivity, ϵ_r (also called relative permittivity), represents the ratio of a materials permittivity to that of free space, ϵ_0 . Dielectric permittivity has been used by past researchers to estimate or relate with moisture contents of different materials like soil (Calabia et al., 2020; Salam et al. 2019), forest litter or woody materials (Razafindratsima et al., 2017; Mai et al., 2015), and of construction materials, such as concrete (Kalogeropoulos, 2011; Kaplanvural, 2023; Dinh et al., 2021) and pavements (Cao & Qadi, 2022). Relevant studies in this context have all showcased the strong correlation between a material's moisture content and its dielectric permittivity and that dielectric permittivity measurement is an alternative means to measure moisture within a material layer. The term 'permittivity' in this study refers to the 'dielectric permittivity' of a material.

Recent research related to waveform inversion for moisture mapping and other applications has often involved the estimation of parameters through a deterministic inversion process using deterministic optimization like particle swarm optimization (Dai et al., 2021; Qin et al., 2020; Kaplanvural et al., 2020), or genetic algorithm (Godio, 2016). Deterministic inversion processes seek to find the optimal solution within a specific parameter space, typically based on the minimization or maximization of an objective function. However, the optimal solutions provided by deterministic inversions may not always be the most appropriate representation of complex multimodal problems and for real-world data that contains noise. In addition, deterministic inversion focuses only on providing deterministic estimates of the optimal solutions with no indication of uncertainty, and thus, the likelihood of other sub-optimal solutions to the inverse problems is not revealed. Uncertainty-aware estimation is necessary for probabilistic risk assessments involving soil moisture and accumulated surface material.

An example of the application of such uncertainty measures is in wildfire risk assessment, where researchers examine the uncertainty in wildfire modeling, offering insights for fire managers and emphasizing key dimensions of uncertainty (Riley and Thompson, 2016).

This study proposes a methodology for automated estimation of both sub-surface permittivity and depth of the layer of the accumulated material on top through probabilistic GPR waveform inversion. To the best of our knowledge, this study is the first to propose a method for soil moisture estimation in the presence of top layers. Although probabilistic soil moisture retrieval has been reported using satellite data (Arellana et al., 2023), past work has focused on analysis of backscattering from bare soils. We propose the application of Bayesian inference with waveform inversion to yield probabilistic estimates of the subsurface unknowns from active sensing data collected by GPR. The posterior probability distribution of the estimated parameters will provide information about the probability of possible sets of solutions to the inverse problem and the uncertainty related to those solutions. The results of this study allow for the rapid assessment of soil and organic top layer by providing probabilistic estimates that could be used in uncertainty-aware analyses and risk assessments.

2. Methodology

To inspect how a GPR signal changes depending on sub-surface properties like depth, permittivity, and electrical conductivity, assume a transmitter (*Tx*) sends an EM wave, part of which is transmitted through, and the remaining is reflected when it encounters a change in the material property (e.g., the bottom face of the material layer in Figure 1a). The reflected wave is received by the radar receiver (*Rx*). The total time of travel (Δt) of the reflected wave from the transmitter to the receiver, represented by the time difference between the peaks in Figure 1(c), depends on the depth (d) and relative permittivity (ϵ_r). This phenomenon can be utilized to analytically calculate the relative permittivity of the material layer, as shown in Equation 1, where c is the velocity of light (3×10^8 m/s). The change in parameters, including depth, permittivity, and conductivity of the material layer, causes a change in the received signal, as shown in Figure 2.

$$\epsilon_r = \left(\frac{c \times \Delta t}{2d} \right)^2 \quad \text{Equation 1}$$

The signals shown in this figure correspond to the one-layer configuration shown in Figure 1. When only depth increases and all other parameters are constant, the signal peak reflected from the bottom of the layer decreases in amplitude due to attenuation and shifts to the right, which indicates increased travel time (Δt) (Figure 2a). For an increase in relative permittivity, the amplitude of direct arrival decreases, and the reflected signal peak shifts to the right, increasing Δt . And, for an increase in conductivity of the layer, the amplitude of the reflected

wave amplitude decreases. These changes in the received GPR signals can be leveraged to predict the properties of the material layers.

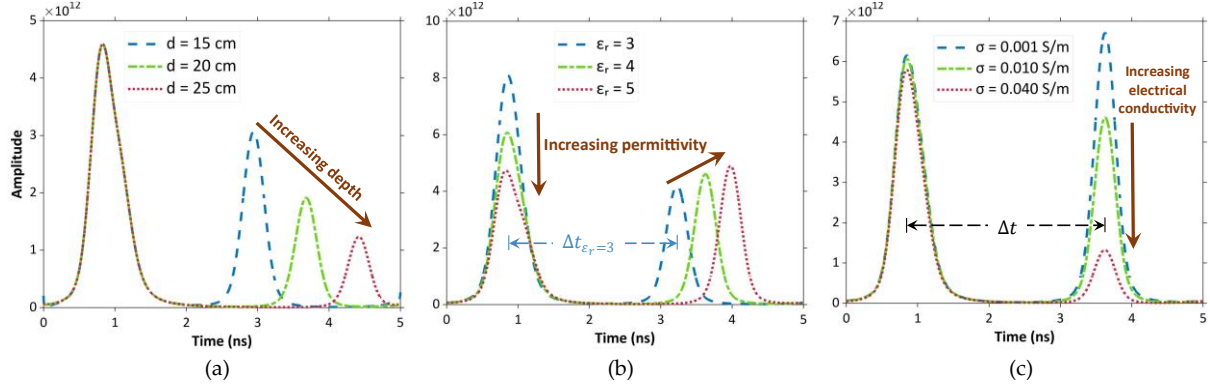


Figure 2: Variation of received GPR signal due to change in layer properties: (a) changing layer depth, (b) changing relative permittivity, (c) changing electrical conductivity.

In this paper, we propose a methodology to leverage the changes in signals to estimate subsurface parameters while accounting for the uncertainties in these estimations. Figure 3 shows the flowchart of the proposed methodology for estimating material parameters using Bayesian model updating. The first step entails the collection of the input radar signal, which can be obtained from a GPR scan. Next, a numerical model is built to simulate electromagnetic wave propagation using the Finite Difference Time Domain (FDTD) technique. The initial parameters of the numerical simulations are random values within a defined range. The model will then be updated by changing the material parameters to match the experimental signal. Model updating can be done by an optimization algorithm, which finds the parameter values by replicating the experimental signal in the numerical simulation.

Deterministic optimization algorithms provide a deterministic estimate, i.e., a single value for each estimated parameter. On the other hand, probabilistic estimates provide increased information about the likelihood and uncertainty related to the estimated values. Hence, Bayesian Model Updating (BMU) was employed to obtain the probabilistic estimate of the optimal values of the parameters of interest. After the BMU analysis, Markov Chain Monte Carlo (MCMC) simulation was used to obtain the posterior distribution of the parameters. At the conclusion of the model-updating process, the numerical response signal obtained by using the most probable values or the mode of the probabilistic estimates more closely matches the experimentally collected GPR A-scan. The estimated permittivity values can be further used to calculate moisture contents by employing empirical equations like Topp's equation (Topp et al., 1980).

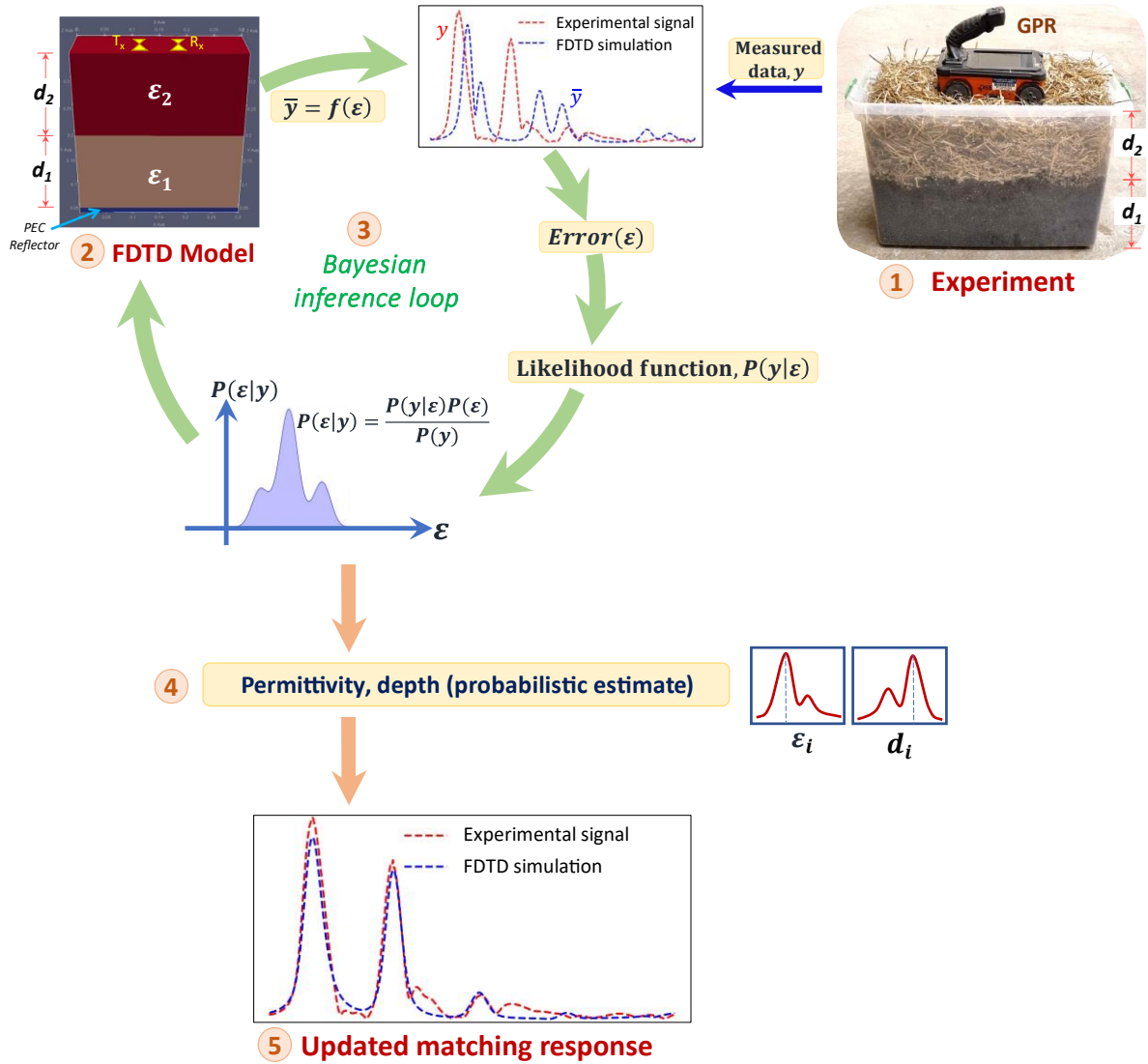


Figure 3: Proposed methodology for parameter estimation.

2.1. FDTD modeling

The finite difference time domain (FDTD) method is useful for solving electromagnetics that have time-dependent phenomena (Mescia et al., 2022; Li et al., 2022). A ground-penetrating radar (GPR) transmits electromagnetic waves through an antenna transmitter and receives the reflected signal through the receiver. To simulate the time-dependent electromagnetic wave propagation phenomena with the underlying physics, the FDTD method has been used in this study. FDTD involves numerically solving Maxwell's equations (set of equations in Equation 2).

$$\begin{aligned}
 \nabla \times E &= -\frac{\partial B}{\partial t} \\
 \nabla \times H &= \frac{\partial D}{\partial t} + J_C + J_S \\
 \nabla \cdot B &= 0 \\
 \nabla \cdot D &= q_v
 \end{aligned} \tag{Equation 2}$$

Where E , B , and H denote the electric field, magnetic field, and magnetic field strength, respectively. The terms D , J , and t also denote electric displacement, current density, volume electric charge density, and time (seconds), respectively. The electric field intensity at the receiver in an FDTD simulation is equivalent to the signal received by a real GPR antenna.

The FDTD method solves Maxwell's equations by discretizing both time and space. The spatial discretization step sizes (Δx , Δy , and Δz) and the temporal step (Δt) are all significant in making the FDTD model more accurate and closer to the true representation. GPR simulations were conducted using an FDTD solver called gprMax (Warren et al., 2016) which has been widely used by many researchers in the past (Liu et al., 2023; Zhang et al., 2022; Qin et al., 2021). Appropriate discretization steps have been chosen after sensitivity analysis to balance the required accuracy with computation time and avoid numerical dispersion. Figure 3 shows an FDTD model of two material layers with a radar transmitter and receiver on the top. Perfectly matched layers (PML) around the geometry (not shown here for clarity) work as absorbent layers that absorb EM waves and represent the characteristics of an open boundary problem.

In order to update and optimize numerical models, a large number of simulations need to be performed within gprMax. Also, the computational demands of simulations using the FDTD technique are significant due to its volumetric nature, necessitating processing time and memory resources. GprMax can execute simulations in graphics processing units (GPUs) using NVIDIA's CUDA framework (Warren et al., 2019), and the high computational power of GPUs can be harnessed to accelerate FDTD simulation in gprMax, offering a way to address the above-mentioned challenges.

2.2. Antenna optimization for simulating real GPR response

To appropriately execute the proposed methodology for real data, simulating the responses of a real GPR is first required through high-fidelity FDTD simulation. An ultra-wideband (UWB) GPR manufactured by GSSI with a listed center frequency of 2700 MHz was used to conduct the experimental investigations (Geophysical Survey Systems, n.d.). The frequency selected for the GPR was considering the focus of this work on surface moisture in the top 15 cm of soil and the ability of high-frequency GPR to determine shallow soil water content (Zhou et al., 2019). According to the manufacturer specifications, the bistatic separation, i.e., the separation between the transmitter and receiver of this GPR, is 6 cm.

An FDTD model was created to accurately simulate the experimental response of this GPR. In most GPR simulations, theoretical sources such as the Hertzian dipole are used as transmitting antennae (Warren & Giannopoulos, 2009). However, the responses obtained from numerical simulation using such theoretical sources do not match accurately with the signals acquired

from real GPR antennas. This is because the simplified theoretical sources do not take into consideration the physical structure and dielectric properties of a real antenna. Some of these parameters of a real antenna are not known or cannot be easily measured (Giannakis et al., 2018). Hence, when numerically modeling real experimental radar investigations, it is customary to model and calibrate the transmitted pulse so that the simulation response closely matches the experimental data (Stadler & Igel, 2022; Warren & Giannopoulos, 2011). Although comprehensive 3D modeling of the antenna structure in FDTD simulation can be conducted for simulating real GPR response, this process requires information not readily supplied by manufacturers. On the contrary, optimizing only the transmitting pulse and its properties would be more convenient and computationally efficient.

In this study, the parameters of the transmitted pulse were optimized prior to the numerical modeling of real GPR signals. The frequency band of the GPR is 0.5-5.0 GHz, within which the center frequency lies. Although the GPR is listed to have a 2.7 GHz antenna, analysis of simple collection scenarios showed significant deviation from this center frequency. Hence, the center frequency was used as a variable parameter to find its optimum value. The second parameter was the type of waveform transmitted by the antenna. The waveforms used for optimization are Gaussian, Gaussiandot, Gaussiandotnorm, and Ricker. The bistatic separation was fixed at 6 cm as per the manufacturer's specifications. The optimum waveform and frequency were found in the simulation by optimization to match the real GPR response.

To perform the antenna optimization, GPR signals were collected in the air for different distances (d) between the GPR and a metallic reflector plate, as shown in Figure 5(a). Two signals for distances of 24 cm and 43 cm were used as experimental responses, and the same setups were modeled in the FDTD simulation to record the numerical response. The metallic reflector was modeled in FDTD simulation as a perfect electrical conductor (PEC). Responses from both experiments and simulations were transformed into amplitude envelopes by applying the Hilbert transform. Bayesian optimization was employed to match the numerical responses to the experimental responses using the objective function (relative error) presented in Equation 3, where y and \bar{y} are respectively, experimental and numerical responses. For the case of the reflector at 24 cm from the GPR, the overlaid responses (amplitude envelopes) before and after optimization are shown in Figure 4. The optimum center frequency was 1.579 GHz, and the optimum waveform type was Gaussian.

$$RE = \sqrt{\frac{\sum(y - \bar{y})^2}{\sum y^2}} \times 100\% \quad \text{Equation 3}$$

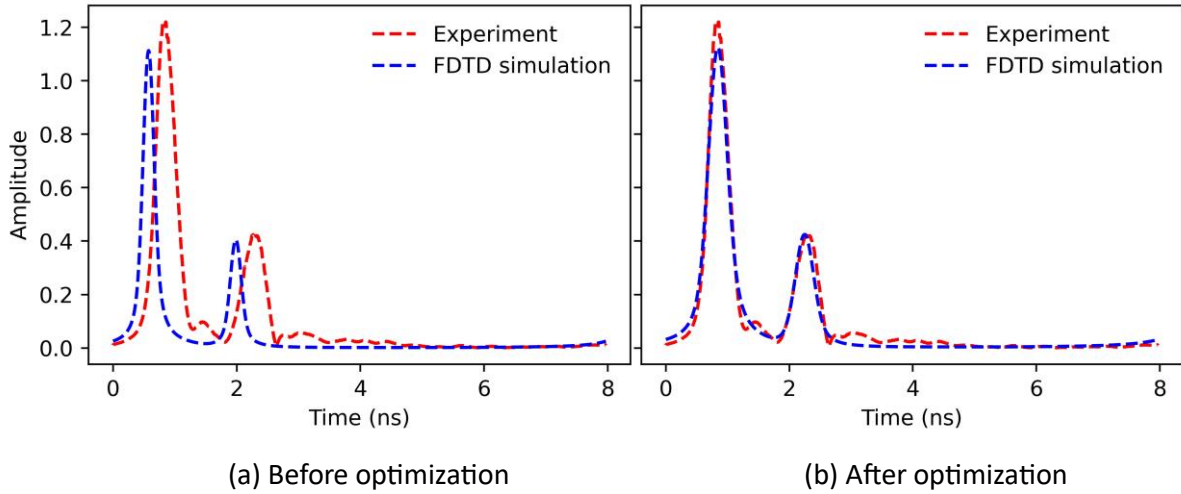


Figure 4: Numerical and experimental response of GPR after antenna optimization.

The performance of the optimized pulse in the simulation was further validated for experimental data collected with metal plate at varying distances from the GPR. Corresponding numerical models were created with the optimized pulse parameters, the metal plate was modeled as a perfect electrical conductor (PEC), and the distance of the PEC from the GPR was predicted by model updating. The predicted distance (or depth) of the metal plate with the optimized antenna pulse parameters are shown against true distance in Figure 5(b), which depicts a good accuracy of prediction. Thus, the optimized pulse parameters were used for further FDTD simulations to model the real GPR used in this study.

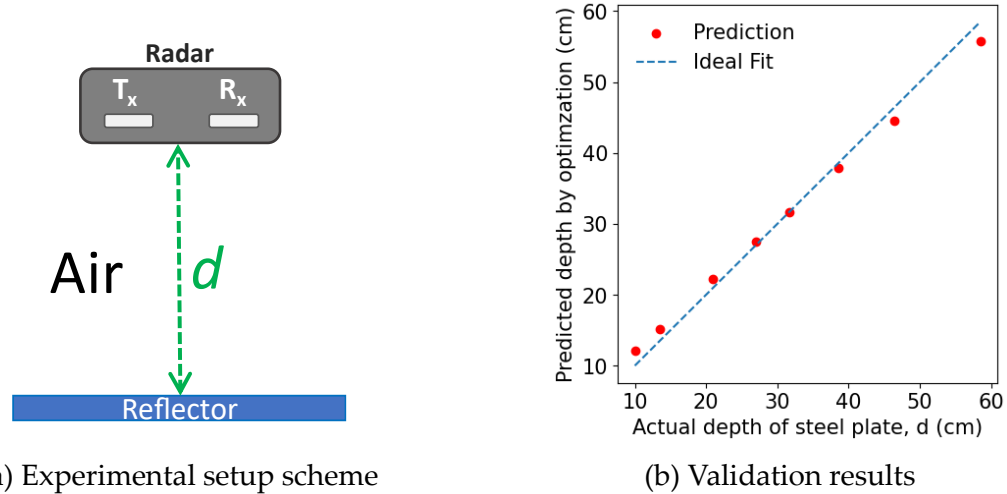


Figure 5: Antenna pulse optimization and validation results.

2.3. Parameter estimation

The process of estimating the parameters includes model updating to match the observed data from the experiments. For instance, in Figure 6, the signals from the numerical simulation initially do not match the experimental signal. The model is updated iteratively by changing the model parameters such as depth and relative permittivity until the two signals match

reasonably. This results in the estimation of the optimal model parameters and finding the model that represents real-world experimental signals with reasonable accuracy.

Model updating-based waveform inversion for parameter estimation is presented using the following two approaches, viz., Bayesian optimization and Bayesian model updating with the MCMC algorithm. Bayesian model updating or Bayesian inference are synonymously used in this paper.

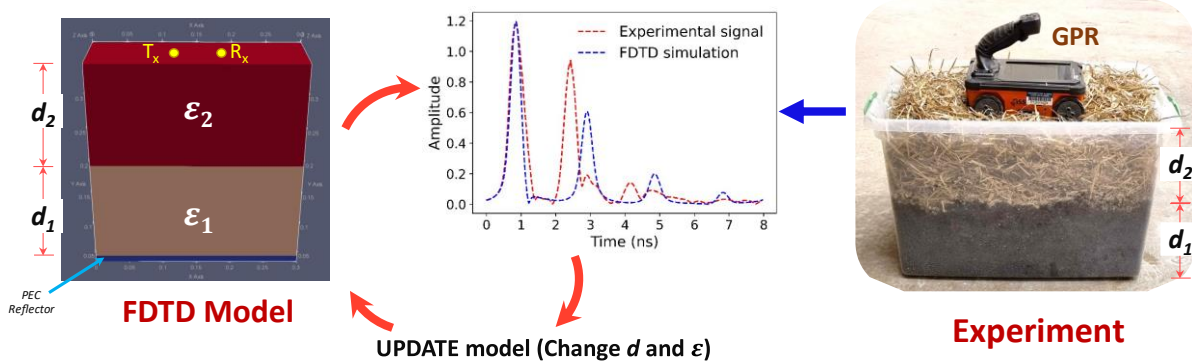


Figure 6: Parameter estimation through model updating.

2.3.1. Bayesian optimization

Initially, the proposed model-updating process was evaluated by estimating the expected values of the parameters of interest such as dielectric permittivity given the measured data (e.g., radar signals) via Bayesian optimization. Bayesian optimization is suitable for evaluating expensive objective functions and in our case, the evaluation of the function requires running expensive FDTD simulations at every iteration. Bayesian optimization operates by creating a Gaussian process-based posterior distribution of functions, aiming to capture the underlying nature of the objective function intended to optimize. As more observations are gathered, this posterior distribution refines itself, enhancing the algorithm's confidence in identifying which unexplored regions are to be further explored. In this paper, the objective function shown in Equation 3 is defined as the relative error (RE) between the experimental and the numerical simulation signal, where the measured signal (y) is from the experiment and \bar{y} is from the FDTD simulation.

2.3.2. Bayesian Model Updating (BMU) using MCMC

Probabilistic Bayesian model updating coupled with Markov Chain Monte Carlo (MCMC) simulation is an efficacious parameter estimation approach, offering several advantages over deterministic optimization methods. First, it allows for incorporating prior knowledge about the modeled system, which is particularly useful in cases with limited data available or where the data could be noisy. Prior knowledge can be obtained from experience or the results of some experiments. Second, it provides a probabilistic framework for model calibration and uncertainty quantification. This means that not only can the model parameters be estimated, but the uncertainty associated with these estimates can also be quantified. This attribute is

pivotal in many applications where the accuracy and reliability of the model are critical. Third, newly available data or evidence can be used to update the model parameters using Bayesian inference, leading to faster optimization of complex and high-dimensional problems.

The schematic representation of the Bayesian model updating (BMU) is shown in the Bayesian inference loop of Figure 3. The measured data (y) is obtained from the GPR experiment, and the experiment is replicated in the FDTD simulation. The FDTD model initialized with random parameters provides \bar{y} which in turn enables the calculation of the error (Equation 4) and the likelihood function. The likelihood is then combined with the prior to provide the posterior distribution of the parameters using Bayes' theorem (Equation 5). In Equation 5, $P(\boldsymbol{\varepsilon}|y)$ is the posterior distribution of the parameters, $P(y|\boldsymbol{\varepsilon})$ is the likelihood, $P(\boldsymbol{\varepsilon})$ is the prior and $P(y)$ is the normalizing term called the evidence. The distribution of dielectric permittivity and other parameters of a material layer is typically unknown before historical data collection programs are conducted. For this reason, a uniform/non-informative prior over the parameter space was assumed in our study. The normalizing term can be ignored, and the inferences about the model parameters can be drawn using Equation 6.

$$\text{Error} = \sqrt{\frac{\sum(y - \bar{y})^2}{\sum y^2}} \quad \text{Equation 4}$$

$$P(\boldsymbol{\varepsilon}|y) = \frac{P(y|\boldsymbol{\varepsilon})P(\boldsymbol{\varepsilon})}{P(y)} \quad \text{Equation 5}$$

$$P(\boldsymbol{\varepsilon}|y) \propto P(y|\boldsymbol{\varepsilon})P(\boldsymbol{\varepsilon}) \quad \text{Equation 6}$$

The GPR data measured through experimental investigation can be described using Equation 7, where $f(\boldsymbol{\varepsilon})$ is the output from non-linear forward simulation and $\text{error}(\boldsymbol{\varepsilon})$ is the measurement data error. To model the likelihood function, the measurement error has been assumed to be independent and normally distributed- $N(0,\sigma)$, with a mean of zero and a constant variance (σ^2). With this formulation, the likelihood function is defined as shown in Equation 8. Here n denotes the number of GPR data samples and σ is the standard deviation of the measurement error). This function was converted to log-likelihood for computational convenience and the log-likelihood function is shown in Equation 9. Better fit between numerical simulation and experimental measurement will result in smaller values of $(f_i(\boldsymbol{\varepsilon}) - y_i)^2$ and larger values of log-likelihood.

As mentioned before, the BMU problem is often solved by Markov Chain Monte Carlo (MCMC) simulation. In MCMC sampling process, a set of criteria that rely solely on the posterior probability density function (PDF) and ignore the normalizing term are used to decide whether to accept or reject the next sample. With the progress of the simulation in each

step, the prior probability density is transformed, and it finally reaches the posterior distribution of each parameter.

$$y = f(\boldsymbol{\varepsilon}) + \text{error}(\boldsymbol{\varepsilon}) \quad \text{Equation 7}$$

$$P(\mathbf{y}|\boldsymbol{\varepsilon}) = \frac{1}{(\sqrt{2\pi}\sigma)^n} \times \exp \left(-\frac{1}{2} \sum_{i=1}^n \left(\frac{f_i(\boldsymbol{\varepsilon}) - y_i}{\sigma} \right)^2 \right) \quad \text{Equation 8}$$

$$P(\mathbf{y}|\boldsymbol{\varepsilon}) = \sum_{i=1}^n \left(-\frac{1}{2} \left(\frac{f_i(\boldsymbol{\varepsilon}) - y_i}{\sigma} \right)^2 - \log \sqrt{2\pi}\sigma \right) \quad \text{Equation 9}$$

2.4. Evaluation of estimated parameters

2.4.1. Time-domain reflectometry (TDR)

To compare the permittivity estimated by model updating, permittivity was also measured by a method called Time-Domain Reflectometry (TDR). TDR measures the time taken for an electromagnetic pulse to travel through a medium and is widely used to calculate the volumetric water content of soil and its bulk dielectric constant or relative permittivity (Topp et al., 1980, Wyseure et al., 1997).

A TDR sensor was used in this study to measure the permittivity and corresponding moisture content of a soil sample. As shown in Figure 7, the sensor probe needs to be inserted into the soil, after which it provides a raw value based on the soil dielectric permittivity. The raw value can then be converted to volumetric water content and relative permittivity by applying the calibration equations of the sensor. The TDR permittivity estimates were then compared to the permittivity values predicted by model updating to check the correlation between them.



Figure 7: Measuring moisture content and permittivity by TDR.

2.4.2. Gravimetric tests

The moisture content of soil can be determined by gravimetric tests (by oven drying). In this process, oven drying of a soil sample is first carried out to determine the mass water content of the soil. Then, the mass water content (MWC) is multiplied by the bulk density of the soil to obtain the volumetric water content (VWC). An estimation of the permittivity can then be obtained from VWC using Topp's equation shown in Equation 10 (Wu et al., 2022; Topp et al., 1980).

$$VWC = -0.053 + 0.0292\epsilon_r - 5.5 \times 10^{-4}\epsilon_r^2 + 4.3 \times 10^{-6}\epsilon_r^3 \quad \text{Equation 10}$$

where ϵ_r denotes the dielectric permittivity.

3. Experimental investigation and results

This section presents the application of the proposed methodology for data collected from experimental investigations.

3.1. Laboratory investigation

The details of the experimental setup are shown in Figure 8. Two layers of material are shown in the setup, namely a bottom soil layer with a depth of d_1 , and an organic top layer having a depth equal to d_2 . The soil layer thickness (d_1) was kept at 15 cm throughout all the experiments. A steel reflector was placed underneath the soil layer (the reflector is shown in the schematic view). The experimental program was designed to validate the proposed methodology for the estimation of soil permittivity soil in bare soil with no layer on top of the soil as well as in soil covered with a layer of organic material. Three different materials with three different coarseness were used as the top layer. These three materials are wood shavings, straw, and wood chips, with average particle sizes of 2.5 mm, 6.4 mm, and 11.7 mm, respectively. GPR scans were recorded from the top of the material on the surface. These experiments were repeated for three different thicknesses of the top layer ($d_2 = 5$ cm, 10 cm, and 15 cm). The estimation of soil permittivity and moisture in the presence of the top layer is analogous to measuring field soil moisture having a woody litter layer on top of the soil.

For all of the different soil/top-layer configurations, experimental data were collected for varying soil moisture contents. To summarize, four different total depths were used: 15 cm soil, 15 cm soil + 5 cm top layer, 15 cm soil + 10 cm top layer, and 15 cm soil + 15 cm top layer; three different top layer materials (straw, wood shaving, and wood chips) were used; and these were repeated for an average of 7 different moisture contents. Hence, the total number of GPR scans collected from the laboratory investigations was 84 (4 depths x 3 top layers x 7 moisture levels).

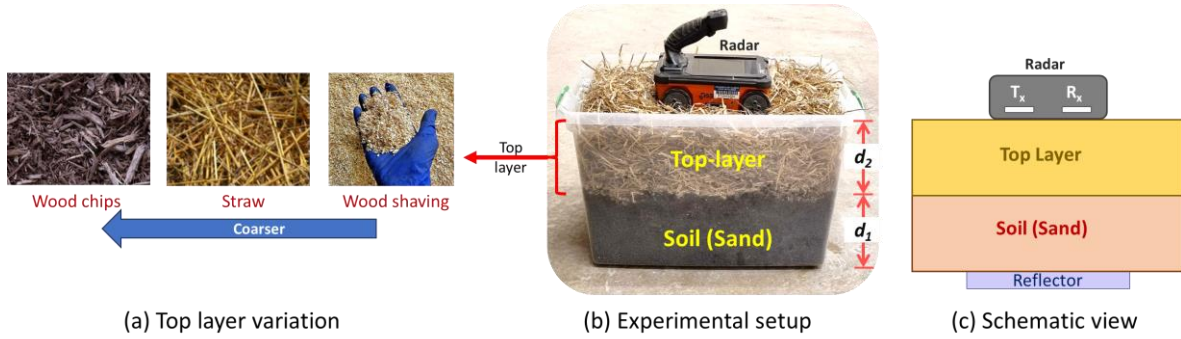


Figure 8: Details of the experimental setup.

3.1.1. Estimation of permittivity

This section demonstrates the estimation of the permittivity of the soil layer using Bayesian optimization. The only model parameters estimated here are the dielectric permittivities of the soil and the top layer. Other parameters, including the depth of the two layers, were assumed to be known and kept constant in the model updating process.

The permittivity predicted by performing a GPR scan and optimization-based model updating is compared with the permittivity estimated by the TDR sensor, and the correlation between the two measurements is shown in Figure 9 for both soil-only and soil-plus top-layer cases. In every case, the lowest R values are reported for the 15 cm soil + 15 cm top layer configuration. This is because there is higher attenuation due to the increased depth of the material, thus deteriorating the predictions for this configuration. The correlation also gets weaker as the average particle size of the top layer increases (wood chips have the largest average particle size), which is due to the attenuation and scattering of EM waves from coarser particles. The reasons for the deterioration of these correlations are better explained by the proposed probabilistic framework of this study, presented in a later section.

3.1.1.1. Correlation with analytical permittivity

The predicted permittivity values were compared with the analytical values estimated by the travel-time method (Equation 1). The correlation for two such cases is shown in Figure 10. The predicted values by model updating have the same trend and strong correlation with the analytical values. However, for accurately calculating analytical permittivity, choosing the correct peak and the time of arrival of that peak is essential. This is subject to subjective interpretation and requires an adequate understanding of the signal. In addition, when the peak from the bottom layer is not strong enough due to attenuation, accurate identification of its time of arrival becomes more challenging, if not impossible. A small deviation from picking the correct time of arrival can lead to a substantial error in permittivity estimation, as permittivity is proportional to the square of the time of flight. Besides, when multiple parameters like permittivity and depth need to be estimated simultaneously, the analytical method will not suffice. These limitations can be overcome by the automated model updating-based parameter estimation proposed in this study.

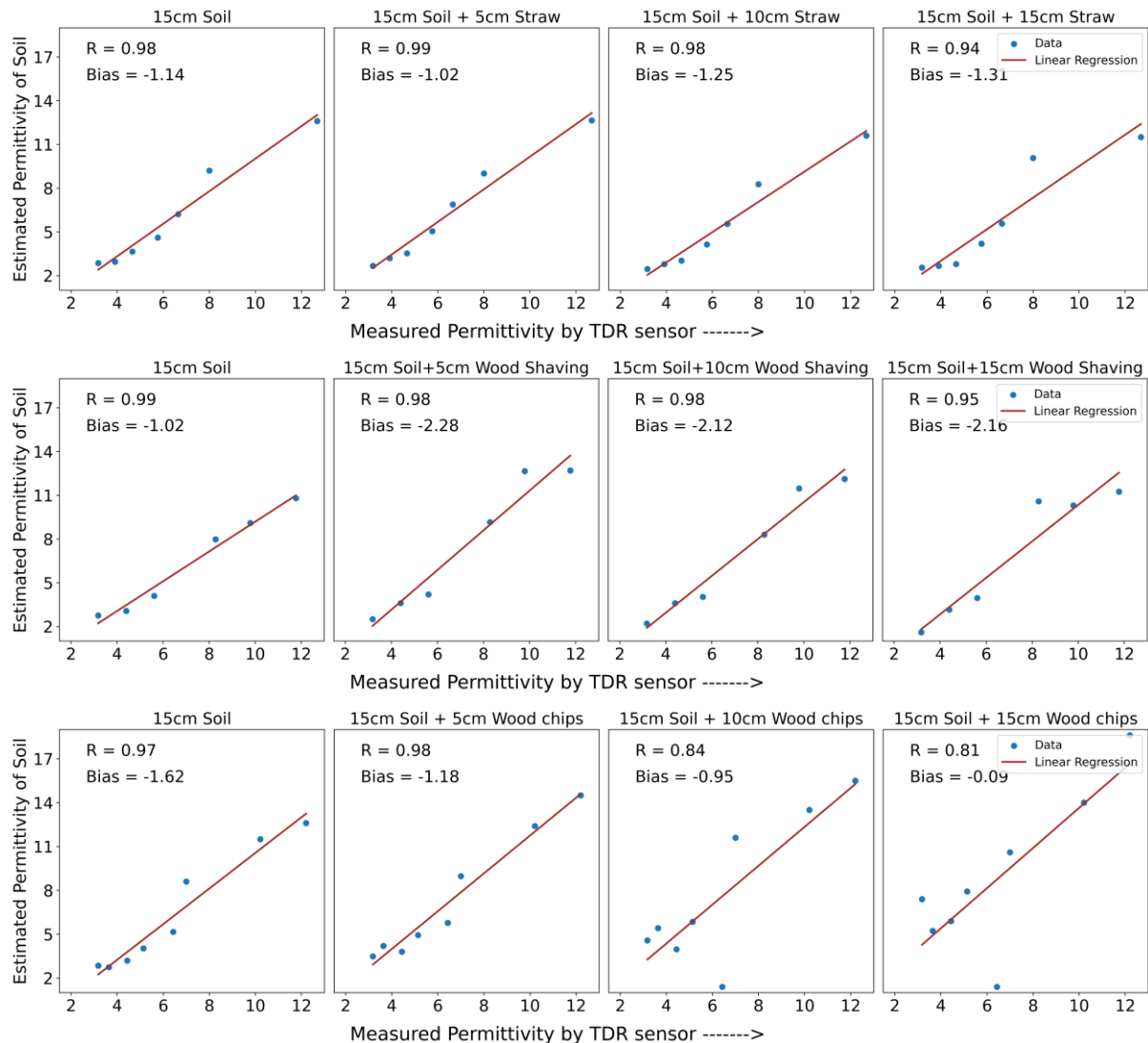


Figure 9: Correlation between estimated (predictions) and measured (TDR) permittivity with permittivity as the only model parameter.

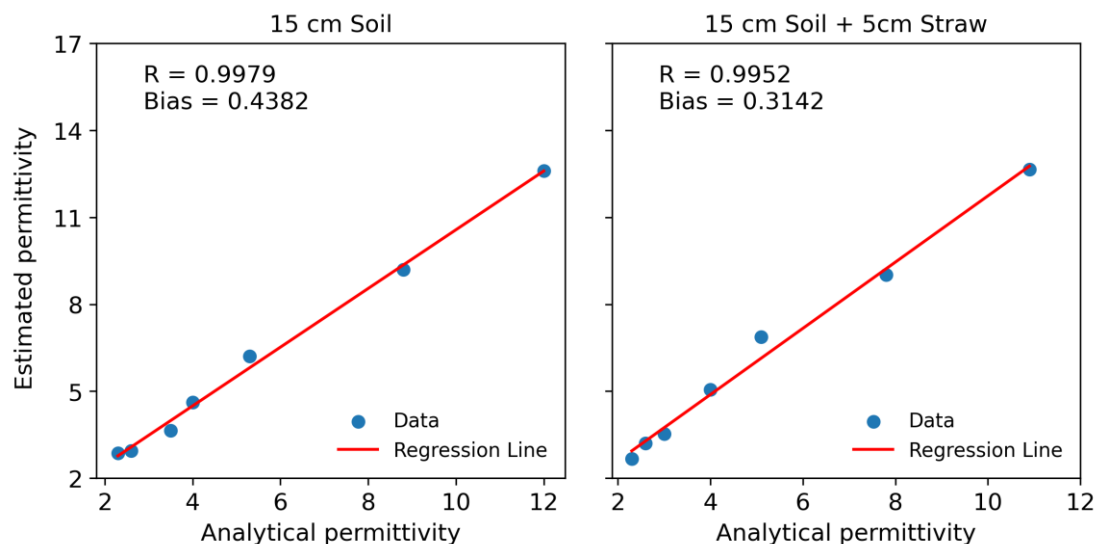


Figure 10: Correlation of estimated permittivity with analytical permittivity.

3.1.2. Estimation of permittivity and top layer depth

When soil moisture sensing is conducted using a reflector, the total depth from the radar at the top to the reflector at the bottom can usually be assumed to be known. However, the amount of material accumulated above the soil, i.e., the top layer depth, remains unknown due to its variation over time. Estimation of this top layer depth can also indicate where along the depth the soil layer begins. Estimating the soil permittivity and the layer depth simultaneously cannot be done by traditional analytical methods from a single GPR A-scan. However, the proposed methodology was employed while keeping multiple parameters as variables in the optimization algorithm. These parameters are the dielectric permittivity, electrical conductivity, and the top layer depth. After performing Bayesian optimization, the predicted permittivities of the soil layer in relation to the measured TDR permittivities are shown in Figure 11. This figure shows good correlations between the measured and estimated permittivities. However, the overall correlations decreased from the case when only permittivity was kept as the variable model parameter for prediction. This is because the current case estimates five parameters instead of two in the previous case, which increases the dimensionality and complexity of the inverse problem. In addition, Figure 11 also shows that the predictions demonstrate a diminished correlation with an increase in top-layer material thickness. This can be associated with an increase in signal attenuation with the increase in material depth, thus resulting in weakened permittivity retrieval. Furthermore, the value of R for (15 cm soil + 15 cm wood chips) was negative, which indicates poor correlation and predictions for this specific case. Such anomalous predictions can be reasonably identified by leveraging probability distributions of the parameters that depict the uncertainty related to the estimates, as will be discussed in a later section.

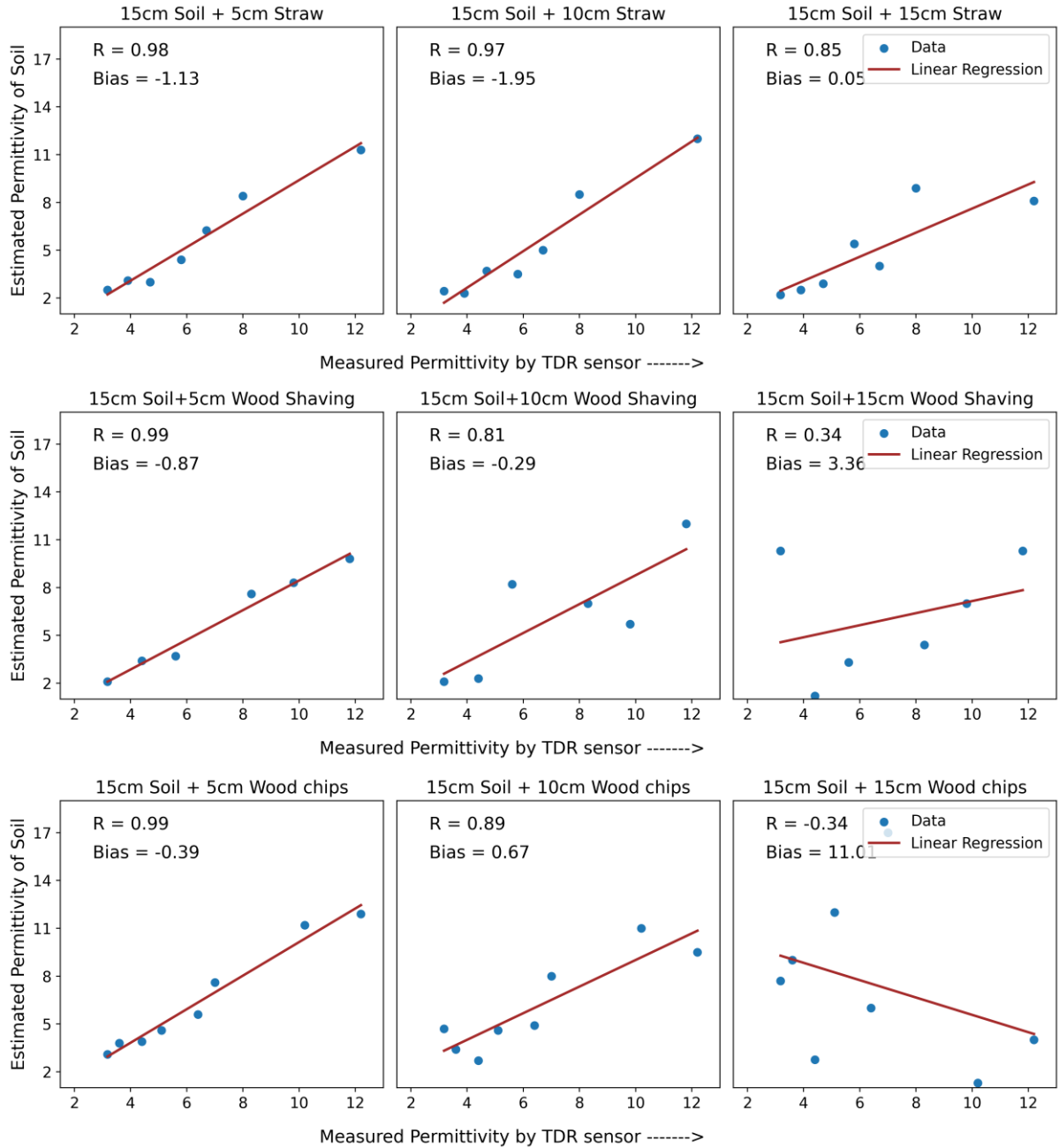


Figure 11: Correlation between estimated (predictions) and measured (TDR) permittivity with variables.

The top layer depth was also predicted by the algorithm, and the summary of the predicted depths for all the experiments is shown with mean and standard deviation in Figure 12. The predicted depths are in reasonable agreement with the true depths, indicating the effectiveness of the method in determining top layer depth along with soil permittivity. For 15 cm wood chips, the error and the standard deviation of predictions are both high. This is because wood chips have larger particle sizes, which causes increased scattering and attenuation of the signal, thus resulting in weaker signal reconstruction.

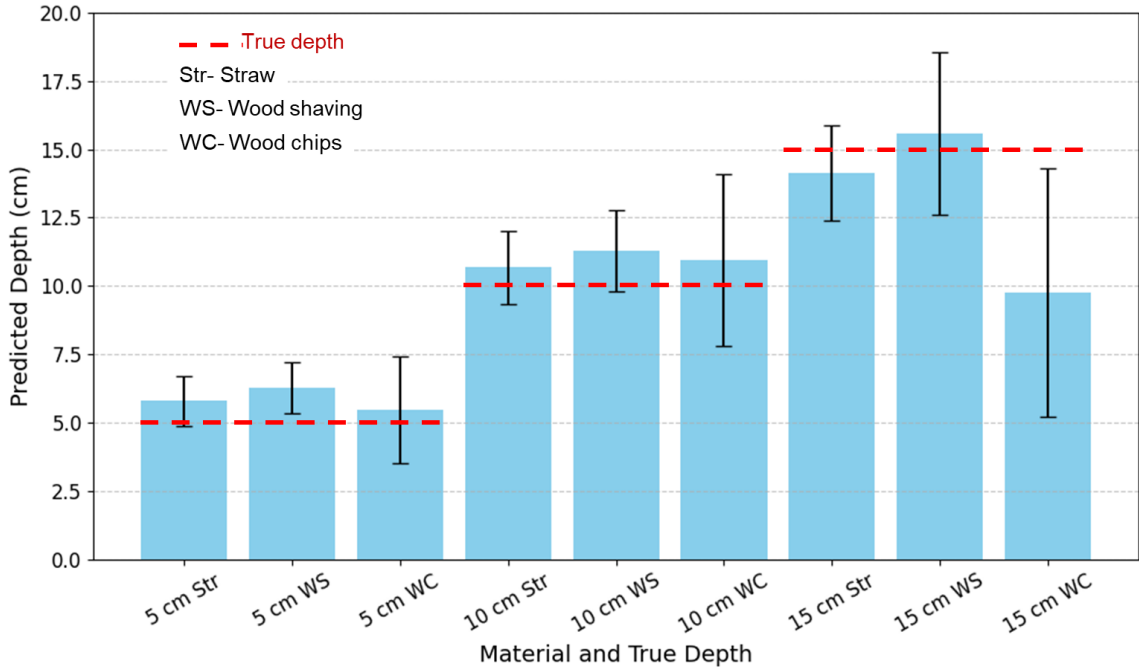


Figure 12: Predicted depth of the top layer material.

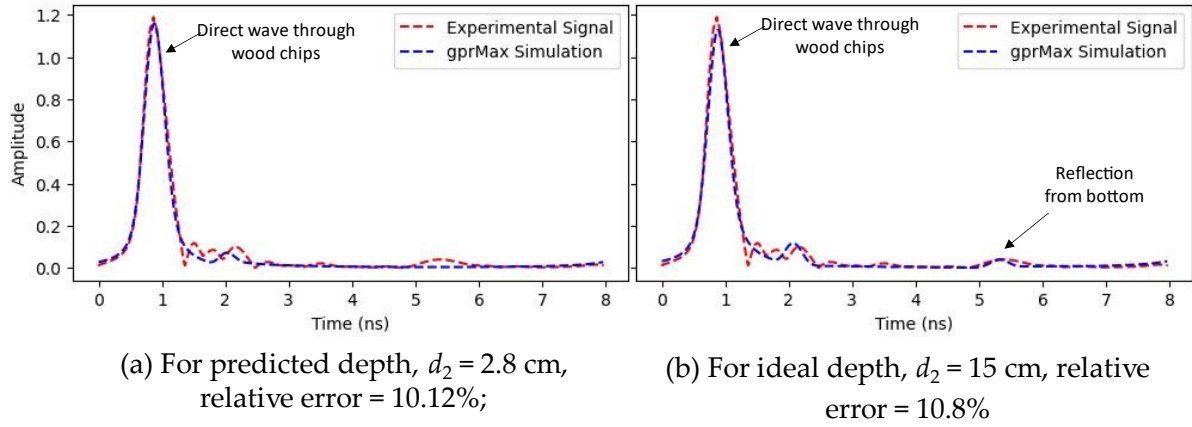


Figure 13: Overlaid plots for (15 cm Soil + 15 cm wood chips) corresponding to TDR soil permittivity of 10.2.

As an illustration, an example from the case of 15 cm soil covered with 15cm wood chips is demonstrated in Figure 13. In this case, the minimum objective function (relative error) results from a top layer depth equal to 2.8 cm, which is significantly smaller than the true depth of 15 cm. Figure 13 shows a comparison between the signal match using the true depth of 15cm (Figure 13b), with that using 2.8 cm (Figure 13a). It shows that the reflection from the bottom is not significant enough to influence the objective function of the optimization. This resulted in the value of the objective function being comparable to that from a different layer configuration, hence making the detectability of the true optimal solution impossible. Such high attenuation and reduction in signal strength are observed as both the permittivity and the total depth increase. In these scenarios, using a lower-frequency GPR may produce stronger signal amplitude from deeper layers and should be the subject of future studies. This

is in line with the widely recognized trade-off between the frequency of GPR and its penetration depth, which should be considered in determining the range of applicability of permittivity retrieval. Nevertheless, the results of the experiments at lower depths clearly demonstrate the validity of the technique in organic top layer depths up to 10 cm.

3.1.3. Probabilistic estimates

3.1.3.1. Convergence of MCMC simulation

To provide an estimation of the uncertainty involved, the Markov Chain Monte Carlo (MCMC) technique was used to sample from the posterior distribution. Optimum values of the hyperparameters of the algorithm were used to balance computation time and the accuracy and convergence of the algorithm. MCMC diagnostics, including the trace plots, were checked to ensure the convergence of the chains, an example of which is depicted in Figure 14. In this figure, the progression of the chains over iterations (or step number) is shown in five plots corresponding to the five parameters estimated. Each plot here has seventeen chains shown with lines of different colors, illustrating how they explore the parameter space. After sufficient iterations/steps, the chains oscillate around a central value, indicating that they have reached a stationary distribution.

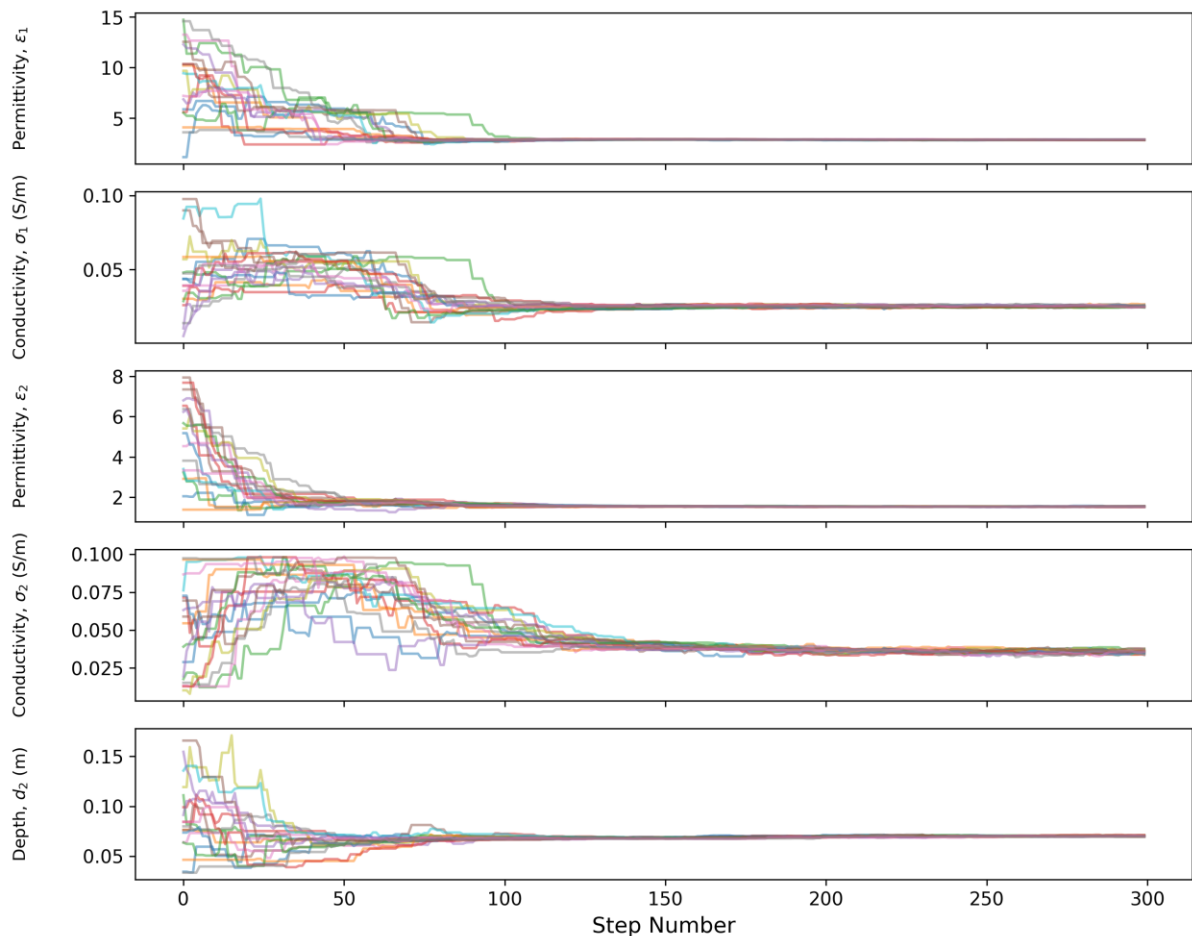


Figure 14: Trace plot showing the convergence of MCMC simulation.

3.1.3.2. Probability distributions of estimated parameters

The posterior distribution of the estimated parameters provides the probability distribution and the uncertainty of the estimated values. The highest probabilities of the parameters were usually observed at the values that were predicted by the Bayesian optimization and presented in the previous section. As an example, the probabilistic estimates for one of the experiments (corresponding to 15 cm soil + 10 cm wood chips), along with their true/measured values, are shown in Figure 15.

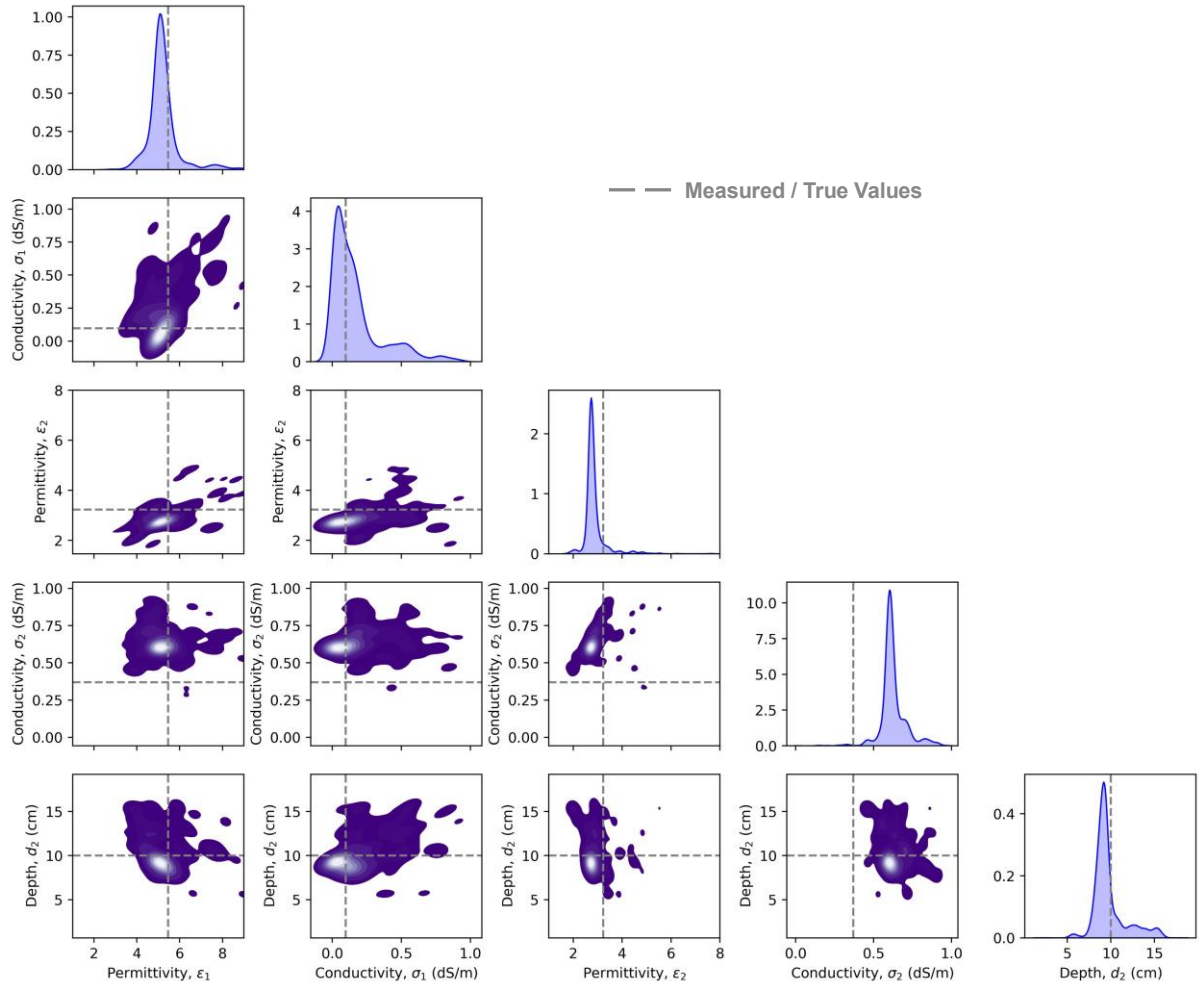


Figure 15: Individual and joint distribution of the estimated parameters.

Five parameters (permittivities and conductivities of the two layers and the depth of the top layer) were estimated by our proposed method, and in this figure, the diagonal plots show the distribution of the individual parameters, and the off-diagonal plot shows the joint distribution of different sets of two parameters. The true depth of the top layer (d_2) was 10cm, and the true soil permittivity (ϵ_1) was estimated to be 5.47. In the absence of direct measurement, this permittivity was found by measuring the water content via gravimetric tests and conversion to permittivity using Topp's equation. The electrical conductivity of both layers and the permittivity of the top layer were estimated by the TDR sensors. From the individual distributions in Figure 15, the maximum-a-posteriori (MAP) value or the mode of

the posterior distribution was observed to be near the true or estimated values. The lighter colors in the joint distributions indicate values of high probability density, and those are mostly observed to be in the vicinity of the true/estimated values. The deviation of the conductivity measurement from the predicted values can be attributed to the limitation of the TDR sensor in measuring the conductivity of coarse woody materials.

3.1.3.3. Uncertainty for different top layer configurations

The distributions of the individual parameters were further inspected to investigate how the top layer configuration affects the prediction in terms of probabilistic confidence and uncertainty. The probability distributions of the predicted soil permittivity are shown in Figure 16 for two variables, viz., depth of the top layer (Figure 16a) and particle size of the top layer material (Figure 16b). As the depth of the top layer decreases, the probability distribution curve shows a higher probability density at the expected value and a narrower spread that indicates lower standard deviation and higher confidence in the prediction. This can be explained by the fact that as the layer depth decreases, there is lower attenuation and the reflection from the reflector is stronger, rendering more information in the signal received by the GPR. Similarly, for higher values of top-layer depth, the signal carries less information due to higher attenuation, which leads to a prediction with lower confidence. This attenuation of signal due to increasing layer depth is also evident in our preliminary investigation on signal variations due to changes in material parameters (Figure 2a).

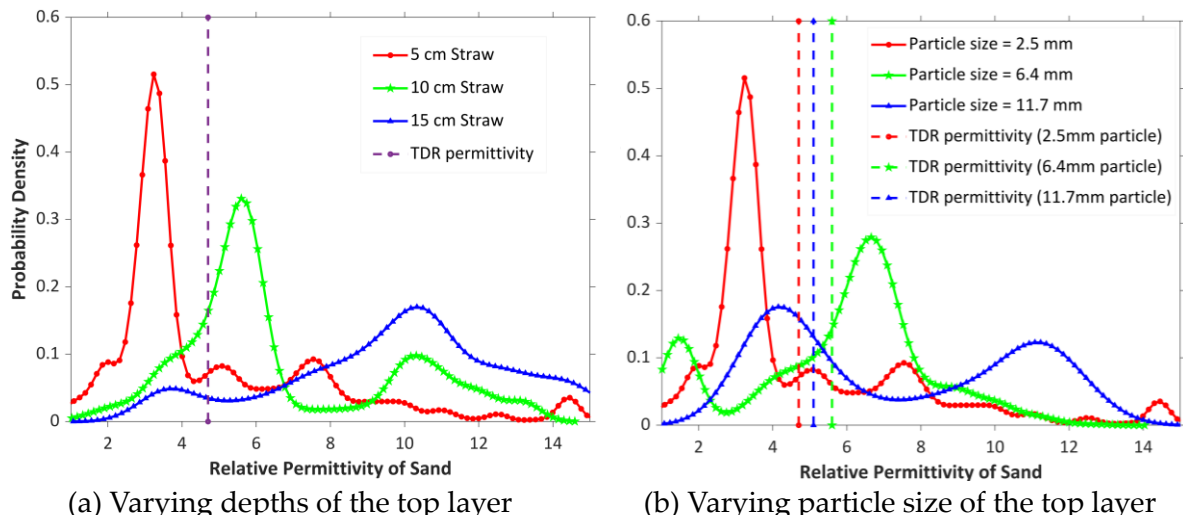


Figure 16: Distributions of estimated permittivity for varying top layer depth and particle size.

A similar phenomenon can be observed in the case of varying particle sizes of the top layer. As the particle size increases, there is more noise and scattering from the coarser particles and, thus, higher attenuation in the received signal. This leads to predictions with lower confidence levels and higher standard deviations. It can also be observed in Figure 16 that the peak value for 15 cm straw depth and the second peak (at permittivity ≈ 11.5) for 11.7 mm particle size

significantly differ from the TDR measurements. The second peak represents the value that can produce a close fit between the numerical and the experimental signal, similar to the case shown in Figure 13, where wrong depth prediction yielded a lower mismatch between the two signals. In these cases, the wider distribution and lower probability density achieved by the Bayesian inference indicate higher uncertainty. Thus, lower confidence and higher uncertainty in prediction obtained by the proposed method are indicators that can facilitate the identification of relatively inconsistent predictions like the ones mentioned above.

3.2. Field investigation and results

Field moisture estimation is crucial for validating the proposed methodology in real applications. The methodology proposed in this study was used to measure the moisture content of the soil surface in the field for sixteen days. The location of the measurement was on the east of the Newmark Civil Engineering Lab of the University of Illinois Urbana Champaign (Figure 17a). Permittivity values were predicted by the proposed method and then converted to volumetric moisture contents using the Topp's equation. The moisture contents were also measured with the TDR sensor at the same time as performing the GPR scans, and soil samples on day 14 and day 16 were collected to determine moisture content by gravimetric tests. The comparison of the predicted moisture contents with TDR measurements and gravimetric tests is shown in Figure 17b. The approximate rainfall periods are also shown here, after each of these periods, depicting a steep rise in the moisture content of the soil. The overall trend of the predicted values matches the trend of the TDR measurements, and the moisture contents estimated by the gravimetric tests are also reasonably close to the predicted values. The slight deviation of the gravimetric results can be attributed to the fact that the bulk density of the soil in field conditions and that in the laboratory test were not precisely the same. From these results, it can be concluded that the proposed method can be applied to field moisture estimation.

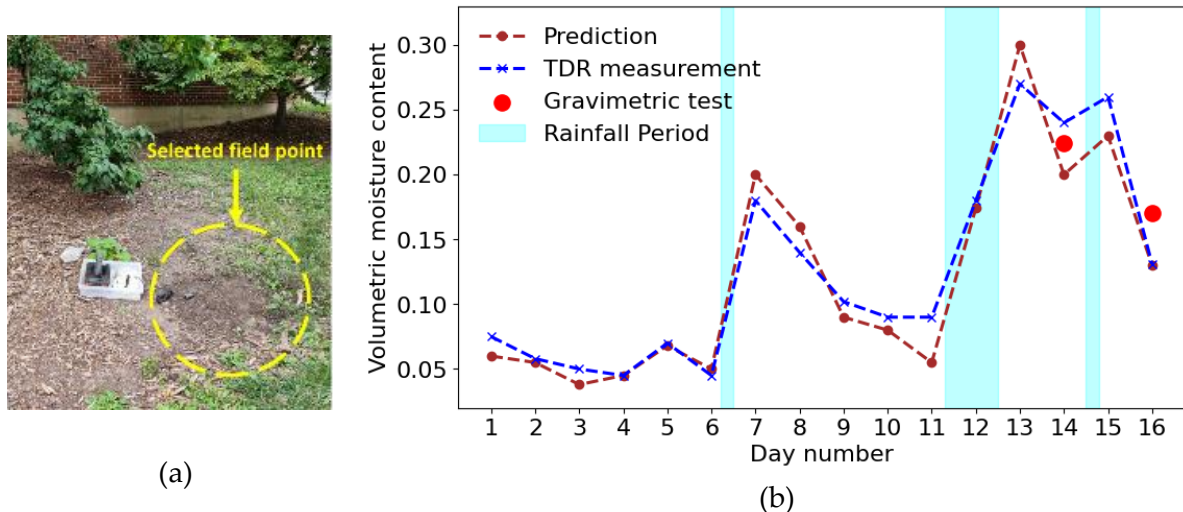


Figure 17: Estimation of field soil moisture content by the proposed method, TDR and gravimetric tests.

4. Limitations and future works

The inconsistent estimations due to attenuation resulting from excessive depth can be associated with the penetration capability or the frequency of the GPR antenna. The discussion to overcome this limitation leads to the well-known tradeoff between resolution and penetration of EM signals as a function of frequency. To harness the strengths of both high and low frequencies, future studies can focus on the simultaneous inclusion of multiple frequencies. This can also help remedy the problem of non-uniqueness in optimization. In addition, while the current study focuses on time-domain signals only, future studies can combine time-domain signal, frequency, and power spectra for more robust parameter estimation. The feasibility and robustness of the proposed parameter estimation for multiple layers can also enable material characterization in more complex applications such as understory ground layer estimations from radars mounted on above-canopy Uncrewed Aerial Systems (UAS). The current method can also be extended for application to data collected by a moving radar like that mounted on a UAS.

5. Conclusions

This paper proposes a Bayesian inversion-based model-updating methodology to estimate sub-surface properties, including depth, dielectric permittivity, and electrical conductivity of layers of material. Model updating was performed through FDTD simulations, and the methodology was validated on experimental data from laboratory and field investigations. The parameters of the transmitted radar pulse in FDTD simulation were first optimized and calibrated, after which FDTD simulations could closely replicate real experimental signals collected by a commercial GPR. Laboratory investigations were carried out to predict permittivities of both bare soil and soil with an overlaying organic material layer having varying levels of coarseness. Field soil moisture was also predicted for sixteen days with the proposed method. The predictions were correlated and compared with measurements obtained by TDR and gravimetric tests. The following conclusions can be drawn from the investigations:

- The proposed method can simultaneously estimate multiple parameters of material layers, including depth, permittivity, and conductivity from GPR signals, while traditional analytical method can only estimate a single parameter (e.g., permittivity) assuming other parameters are known (e.g., depth).
- The proposed method can provide probabilistic estimates of sub-surface permittivity, moisture content, conductivity, and depth using Bayesian inference with the MCMC algorithm. The probabilistic predictions provide the distribution of the estimated parameters and the uncertainty related to those predictions.
- The predictions in the laboratory investigations are in good agreement with TDR measurements for bare soil and soil with an overlaying material layer of up to 10 cm

depth. Predicted soil permittivity or water content is also in good agreement with values estimated by gravimetric tests.

- For higher depth (> 10 cm) and coarser particle size of the top layer material, the attenuation of the received GPR signal results in inconsistent permittivity predictions and diminished correlation with TDR measurements. However, these inconsistent predictions showed lower probability density and larger standard deviation, indicating higher uncertainty compared to the accurate predictions. As such, the proposed uncertainty estimation method can be leveraged to identify such inconsistent predictions.
- The predicted field soil moisture content is also in good agreement with the trend of the TDR measurements and moisture content measured by gravimetric tests, validating the effectiveness of the proposed method for field moisture estimation.

Overall, it was shown that the proposed method can estimate sub-surface depth, dielectric permittivity, and moisture content, which can be used for a wide range of applications spanning precision agriculture, environmental sensing, and moisture mapping to wildfire risk assessment and non-destructive evaluation (NDE) in engineering structures.

Acknowledgments

This study was in part funded by the United States Forest Service and Keysight Technologies. The authors sincerely appreciate this support. The authors would also like to express their sincere appreciation to the NVIDIA Corporation for their generous support with the donation of GPUs used in this study. The authors also sincerely thank Yuxiang Zhao and Kurt Soncco for assistance with computing and simulation, Anshu Abhinav for assistance with TDR operation, and Coleman Froehlke for assistance during data collection and gravimetric tests. The authors further thank Matthew Ware and the GSSI technical team for their technical support.

Data and code availability

The Python code used to generate the findings of this study is available in the following GitHub repository: <https://github.com/ishfaqa2/Code-Bayesian-Inversion-of-GPR-waveforms->. A sample of the experimental data is also available at the same repository.

References

Alipour, M., La Puma, I., Picotte, J., Shamsaei, K., Rowell, E., Watts, A., Kosovic, B., Ebrahimian, H., & Taciroglu, E. (2023). A Multimodal Data Fusion and Deep Learning Framework for Large-Scale Wildfire Surface Fuel Mapping. *Fire*, 6(2), 36. <https://doi.org/10.3390/fire6020036>

Arellana, J., Franco, M., & Grings, F. (2023). Using SAOCOM data and Bayesian Inference to estimate soil dielectric constant in agricultural soils. *IEEE Geoscience and Remote Sensing Letters*. <https://doi.org/10.1109/LGRS.2023.3296094>

Brandt, O., Langley, K., Kohler, J., & Hamran, S. E. (2007). Detection of buried ice and sediment layers in permafrost using multi-frequency Ground Penetrating Radar: A case examination on Svalbard. *Remote Sensing of Environment*, 111(2-3), 212-227.

Calabia, A., Molina, I., & Jin, S. (2020). Soil Moisture Content from GNSS Reflectometry Using Dielectric Permittivity from Fresnel Reflection Coefficients. *Remote Sensing*, 12(1), 122. <https://doi.org/10.3390/rs12010122>

Cao, Q., & Al-Qadi, I. L. (2021). Effect of moisture content on calculated dielectric properties of asphalt concrete pavements from ground-penetrating radar measurements. *Remote Sensing*, 14(1), 34. <https://doi.org/10.3390/rs14010034>

Cova, G. R., Prichard, S. J., Rowell, E., Drye, B., Eagle, P., Kennedy, M. C., & Nemens, D. G. (2023). Evaluating Close-Range Photogrammetry for 3D Understory Fuel Characterization and Biomass Prediction in Pine Forests. *Remote Sensing*, 15(19), 4837. <https://doi.org/10.3390/rs15194837>

Dai, Q., Zhang, H., & Zhang, B. (2021). An improved particle swarm optimization based on total variation regularization and projection constraint with applications in ground-penetrating radar inversion: A model simulation study. *Remote Sensing*, 13(13), 2514.

Dinh, T. T., Hegler, S., Liebscher, M., Navarro de Sosa, I., Li, H., Plettemeier, D., Drossel, W., & Mechtcherine, V. (2021). Dielectric material characterization of concrete in GHz range in dependence on pore volume and water content. *Construction and Building Materials*, 311, 125234. <https://doi.org/10.1016/j.conbuildmat.2021.125234>

Dunn, P. H., Barro, S. C., & Poth, M. (1985). Soil moisture affects survival of microorganisms in heated chaparral soil. *Soil Biology and Biochemistry*, 17(2), 143-148. [https://doi.org/10.1016/0038-0717\(85\)90105-1](https://doi.org/10.1016/0038-0717(85)90105-1)

Falkowski, M. J., Gessler, P. E., Morgan, P., Hudak, A. T., & Smith, A. M. (2005). Characterizing and mapping forest fire fuels using ASTER imagery and gradient modeling. *Forest Ecology and Management*, 217(2-3), 129-146. <https://doi.org/10.1016/j.foreco.2005.06.013>

Feng, D., Liu, Y., Wang, X., Zhang, B., Ding, S., Yu, T., Li, B., & Feng, Z. (2023). Inspection and Imaging of Tree Trunk Defects Using GPR Multifrequency Full-Waveform Dual-Parameter Inversion. *IEEE Transactions on Geoscience and Remote Sensing*, 61, 1-15.

Feng, D., Wang, X., & Zhang, B. (2019). Improving reconstruction of tunnel lining defects from ground-penetrating radar profiles by multi-scale inversion and bi-parametric full-waveform inversion. *Advanced Engineering Informatics*, 41, 100931.

García, M., Riaño, D., Yebra, M., Salas, J., Cardil, A., Monedero, S., Ramirez, J., Martín, M. P., Vilar, L., Gajardo, J., & Ustin, S. (2020). A Live Fuel Moisture Content Product from Landsat TM Satellite Time Series for Implementation in Fire Behavior Models. *Remote Sensing*, 12(11), 1714. <https://doi.org/10.3390/rs12111714>

Geophysical Survey Systems. (n.d.). MINIXT the StructureScan Mini XT is a GPR handheld analyzer test report revision history. <https://fccid.io/QF7MINIXT/Test-Report/Test-Report-2883301> (accessed 11.19.23).

Giannakis, I., Giannopoulos, A., & Warren, C. (2018). Realistic FDTD GPR antenna models optimized using a novel linear/nonlinear full-waveform inversion. *IEEE Transactions on Geoscience and Remote Sensing*, 57(3), 1768-1778. <https://doi.org/10.1109/TGRS.2018.2869027>

Godio, A. (2016). Multi population genetic algorithm to estimate snow properties from GPR data. *Journal of Applied Geophysics*, 131, 133-144.

Haruzi, P., Schmäck, J., Zhou, Z., van der Kruk, J., Vereecken, H., Vanderborght, J., & Klotzsche, A. (2022). Detection of Tracer Plumes Using Full-Waveform Inversion of Time-Lapse Ground Penetrating Radar Data: A Numerical Study in a High-Resolution Aquifer Model. *Water Resources Research*, 58(5), e2021WR030110.

He, R., Nantung, T., Olek, J., & Lu, N. (2023). Field study of the dielectric constant of concrete: A parameter less sensitive to environmental variations than electrical resistivity. *Journal of Building Engineering*, 74, 106938. <https://doi.org/10.1016/j.jobe.2023.106938>

Jensen, D., Reager, J. T., Zajic, B., Rousseau, N., Rodell, M., & Hinkley, E. (2018). The sensitivity of US wildfire occurrence to pre-season soil moisture conditions across ecosystems. *Environmental Research Letters*, 13(1), 014021. <https://doi.org/10.1088/1748-9326/aa9853>

Josephson, C., Kotaru, M., Weinstein, K., Katti, S., & Chandra, R. (2021, June). Low-cost in-ground soil moisture sensing with radar backscatter tags. In ACM SIGCAS conference on computing and sustainable societies (pp. 299-311). <https://doi.org/10.1145/3460112.3472326>

Kalogeropoulos, A., Van der Kruk, J., Hugenschmidt, J., Busch, S., & Merz, K. (2011). Chlorides and moisture assessment in concrete by GPR full waveform inversion. *Near Surface Geophysics*, 9(3), 277-286.

Kaplanvural, İ. (2023). Volumetric water content estimation of concrete by particle swarm optimization of GPR data. *Construction and Building Materials*, 375, 130995. <https://doi.org/10.1016/j.conbuildmat.2023.130995>

Kaplanvural, İ., Pekşen, E., & Özkap, K. (2020). 1D waveform inversion of GPR trace by particle swarm optimization. *Journal of Applied Geophysics*, 181, 104157.

Klewe, T., Strangfeld, C., & Kruschwitz, S. (2021). Review of moisture measurements in civil engineering with ground penetrating radar – Applied methods and signal features. *Construction and Building Materials*, 278, 122250. <https://doi.org/10.1016/j.conbuildmat.2021.122250>

Krueger, E. S., Ochsner, T. E., Engle, D. M., Carlson, J. D., Twidwell, D., & Fuhlendorf, S. D. (2015). Soil Moisture Affects Growing-Season Wildfire Size in the Southern Great Plains. *Soil Science Society of America Journal*, 79(6), 1567-1576. <https://doi.org/10.2136/sssaj2015.01.0041>

Li, Y., Liu, C., Yue, G., Gao, Q., & Du, Y. (2022). Deep learning-based pavement subsurface distress detection via ground penetrating radar data. *Automation in Construction*, 142, 104516.

Liu, X., Dong, X., & Leskovar, D. I. (2016). Ground penetrating radar for underground sensing in agriculture: a review. *International Agrophysics*, 30(4).

Liu, Z., Yeoh, J. K., Gu, X., Dong, Q., Chen, Y., Wu, W., Wang, L., & Wang, D.. (2023). Automatic pixel-level detection of vertical cracks in asphalt pavement based on GPR investigation and improved mask R-CNN. *Automation in Construction*, 146, 104689.

Mai, T. C., Razafindratsima, S., Sbartaï, Z. M., Demontoux, F., & Bos, F. (2015). Non-destructive evaluation of moisture content of wood material at GPR frequency. *Construction and Building Materials*, 77, 213-217. <https://doi.org/10.1016/j.conbuildmat.2014.12.030>

Mescia, L., Bia, P., & Caratelli, D. (2022). FDTD-based electromagnetic modeling of dielectric materials with fractional dispersive response. *Electronics*, 11(10), 1588. <https://doi.org/10.3390/electronics11101588>

Mutlu, M., Popescu, S. C., & Zhao, K. (2008). Sensitivity analysis of fire behavior modeling with LIDAR-derived surface fuel maps. *Forest Ecology and Management*, 256(3), 289-294. <https://doi.org/10.1016/j.foreco.2008.04.014>

Naderpour, M., Rizeei, H. M., & Ramezani, F. (2021). Forest Fire Risk Prediction: A Spatial Deep Neural Network-Based Framework. *Remote Sensing*, 13(13), 2513. <https://doi.org/10.3390/rs13132513>

Prichard, S. J., Kennedy, M. C., Andreu, A. G., Eagle, P. C., French, N. H., & Billmire, M. (2019). Next-Generation Biomass Mapping for Regional Emissions and Carbon Inventories: Incorporating Uncertainty in Wildland Fuel Characterization. *Journal of Geophysical Research: Biogeosciences*, 124(12), 3699-3716. <https://doi.org/10.1029/2019JG005083>

Qin, H., Zhang, D., Tang, Y., & Wang, Y. (2021). Automatic recognition of tunnel lining elements from GPR images using deep convolutional networks with data augmentation. *Automation in Construction*, 130, 103830.

Qin, T., Zhao, Y., Hu, S., An, C., Bi, W., Ge, S., Capineri, L., & Bohlen, T. (2020). An interactive integrated interpretation of GPR and Rayleigh wave data based on the genetic algorithm. *Surveys in Geophysics*, 41, 549-574.

Rao, K., Williams, A. P., Flefil, J. F., & Konings, A. G. (2020). SAR-enhanced mapping of live fuel moisture content. *Remote Sensing of Environment*, 245, 111797. <https://doi.org/10.1016/j.rse.2020.111797>

Razafindratsima, S., Sbartaï, Z. M., & Demontoux, F. (2017). Permittivity measurement of wood material over a wide range of moisture content. *Wood science and technology*, 51, 1421-1431.

Riley, K., & Thompson, M. (2016). An uncertainty analysis of wildfire modeling. *Natural Hazard Uncertainty Assessment: Modeling and Decision Support*, 191-213. <https://doi.org/10.1002/9781119028116.ch13>

Salam, A., Vuran, M. C., & Irmak, S. (2019). Di-Sense: In situ real-time permittivity estimation and soil moisture sensing using wireless underground communications. *Computer Networks*, 151, 31-41. <https://doi.org/10.1016/j.comnet.2019.01.001>

Serbin, G., & Or, D. (2005). Ground-penetrating radar measurement of crop and surface water content dynamics. *Remote Sensing of Environment*, 96(1), 119-134. <https://doi.org/10.1016/j.rse.2005.01.018>

Shaik, R. U., Alipour, M., & Taciroglu, E. (2023, July). A Bibliometric Analysis of Artificial Intelligence-Based Solutions to Challenges in Wildfire Fuel Mapping. In *IGARSS 2023-2023 IEEE International Geoscience and Remote Sensing Symposium* (pp. 1610-1613). IEEE. <https://doi.org/10.1109/IGARSS52108.2023.10282462>

Sinchi, K. S., Calderon, D., Aziz, I., Watts, A., Soltanaghai, E., & Alipour, M. (2023, July). Under-Canopy Biomass Sensing using UAS-Mounted Radar: a Numerical Feasibility Analysis. In *IGARSS 2023-2023 IEEE International Geoscience and Remote Sensing Symposium* (pp. 3292-3295). IEEE. <https://doi.org/10.1109/IGARSS52108.2023.10282771>

Srivastava, P. K. (2017). Satellite soil moisture: Review of theory and applications in water resources. *Water Resources Management*, 31(10), 3161-3176. <https://doi.org/10.1007/s11269-017-1722-6>

Stadler, S., & Igel, J. (2022). Developing Realistic FDTD GPR Antenna Surrogates by Means of Particle Swarm Optimization. *IEEE Transactions on Antennas and Propagation*, 70(6), 4259–4272. <https://doi.org/10.1109/TAP.2022.3142335>

Stavros, E. N., Coen, J., Peterson, B., Singh, H., Kennedy, K., Ramirez, C., & Schimel, D. (2018). Use of imaging spectroscopy and LIDAR to characterize fuels for fire behavior prediction. *Remote Sensing Applications: Society and Environment*, 11, 41-50. <https://doi.org/10.1016/j.rsase.2018.04.010>

Thomas Ambadan, J., Oja, M., Gedalof, Z., & Berg, A. A. (2020). Satellite-Observed Soil Moisture as an Indicator of Wildfire Risk. *Remote Sensing*, 12(10), 1543. <https://doi.org/10.3390/rs12101543>

Topp, G. C., Davis, J. L., & Annan, A. P. (1980). Electromagnetic determination of soil water content: Measurements in coaxial transmission lines. *Water resources research*, 16(3), 574-582.

Warren, C., & Giannopoulos, A. (2009, June). Optimising models of commercial GPR antennas. In *Proceedings of the 5th International Workshop on Advanced Ground Penetrating Radar* (pp. 18-22). University of Grenada, Grenada, Spain.

Warren, C., & Giannopoulos, A. (2011). Creating finite-difference time-domain models of commercial ground-penetrating radar antennas using Taguchi's optimization method. *Geophysics*, 76(2). <https://doi.org/10.1190/1.3548506>

Warren, C., Giannopoulos, A., & Giannakis, I. (2016). gprMax: Open source software to simulate electromagnetic wave propagation for Ground Penetrating Radar. *Computer Physics Communications*, 209, 163-170.

Warren, C., Giannopoulos, A., Gray, A., Giannakis, I., Patterson, A., Wetter, L., & Hamrah, A. (2019). A CUDA-based GPU engine for gprMax: Open source FDTD electromagnetic simulation software. *Computer Physics Communications*, 237, 208-218.

Wickramanayake, S., Thiyagarajan, K., & Kodagoda, S. (2022). Deep learning for estimating low-range concrete sub-surface boundary depths using ground penetrating radar signals. *IEEE Sensors Letters*, 6(3), 1-4. <https://doi.org/10.1109/LSENS.2022.3147470>

Wu, K., Desesquelles, H., Cockenpot, R., Guyard, L., Cuisiniez, V., & Lambot, S. (2022). Ground-penetrating radar full-wave inversion for soil moisture mapping in Trench-Hill potato fields for precise irrigation. *Remote Sensing*, 14(23), 6046.

Wu, K., Rodriguez, G. A., Zajc, M., Jacquemin, E., Clément, M., De Coster, A., & Lambot, S. (2019). A new drone-borne GPR for soil moisture mapping. *Remote Sensing of Environment*, 235, 111456.

Wyseure, G. C. L., Mojid, M. A., & Malik, M. A. (1997). Measurement of volumetric water content by TDR in saline soils. *European Journal of Soil Science*, 48(2), 347-354. <https://doi.org/10.1111/j.1365-2389.1997.tb00555.x>

Xie, L., Xia, Z., Xue, S., & Fu, X. (2022). Detection of setting time during cement hydration using ground penetrating radar. *Journal of Building Engineering*, 60, 105166.

Yu, Y., Huisman, J. A., Klotzsche, A., Vereecken, H., & Weihermüller, L. (2022). Coupled full-waveform inversion of horizontal borehole ground penetrating radar data to estimate soil hydraulic parameters: A synthetic study. *Journal of Hydrology*, 610, 127817.

Zhang, J., Lu, Y., Yang, Z., Zhu, X., Zheng, T., Liu, X., Tian, Y., & Li, W. (2022). Recognition of void defects in airport runways using ground-penetrating radar and shallow CNN. *Automation in Construction*, 138, 104260. <https://doi.org/10.1016/j.autcon.2022.104260>

Zhou, L., Yu, D., Wang, Z., & Wang, X. (2019). Soil Water Content Estimation Using High-Frequency Ground Penetrating Radar. *Water*, 11(5), 1036. <https://doi.org/10.3390/w11051036>